Title: **Working with Dynamic Earthquake Rupture Models: A Practical Guide**

Authors: Marlon D. Ramos[1,2], Prithvi Thakur[1], Yihe Huang[1], Ruth A. Harris[3], Kenny J. Ryan[2]

1. University of Michigan, Department of Earth and Environmental Sciences
2. Air Force Research Laboratory
3. United States Geological Survey, Moffett Field, California

This preprint is currently under revision at Seismological Research Letters.

Social Media Twitter: @MarlonDRamos1

Working with Dynamic Earthquake Rupture Models: A Practical Guide

Marlon D. Ramos[1,2], Prithvi Thakur[1], Yihe Huang[1], Ruth A. Harris[3], Kenny J. Ryan[2]

1. *University of Michigan, Department of Earth and Environmental Sciences*
2. *Air Force Research Laboratory*
3. *United States Geological Survey, Moffett Field, California*

Corresponding Author:

Marlon D. Ramos
ramosmd@umich.edu
https://orcid.org/0000-0003-4449-8624
Air Force Research Laboratory
3550 Aberdeen Dr SE
Kirtland Air Force Base
Albuquerque, NM 87108

Abstract

Dynamic rupture models are physics-based simulations that couple fracture mechanics to wave propagation and are used to explain specific earthquake observations or to generate a suite of predictions to understand the influence of frictional, geometrical, stress and material parameters. These simulations can model single earthquakes or multiple earthquake cycles. The objective of this paper is to provide a self-contained and practical guide for students starting in the field of earthquake dynamics. Senior researchers who are interested in learning the first order constraints and general approaches to dynamic rupture problems will also benefit. We believe this guide is timely given the recent growth of computational resources and the range of sophisticated modeling software that are now available. We start with a succinct discussion of the essential physics of earthquake rupture propagation and walk the reader through critical concepts in dynamic rupture model design. We briefly touch on fully dynamic earthquake cycle models, but leave the details of this topic for other publications. We also highlight examples throughout that demonstrate the use of dynamic rupture models to investigate various aspects of the faulting process.

1. Introduction

Why do we model earthquakes? Seismology began as an observational science that strove to link the recordings of elastic waves at Earth's surface to physical processes occurring within the interior (Ben-Menahem, 1995). The conceptional framework established by Reid (1911) related earthquakes and the seismic waves they produce to slip along fractures in Earth's lithosphere. Modeling the earthquake rupture process from nucleation to arrest can help us reconcile different hypotheses for how earthquakes release energy and impact hazard. But our ability to use earthquake models is dependent on how we think about the physics of fault rupture and the quality of geologic and geophysical observations used to design the models.

In order to infer the conditions responsible for generating seismic waves, a formal mathematical description of the source is needed. Some of the first earthquake models treated a slipping fault as a point in space (point-source models; Nakano, 1923; Pujol and Herrmann, 1990); provided that observations are made at hypocentral distances much larger than the fault dimensions, this approximation has remained valid. Point-source models show the equivalency between shear fracture dislocation (i.e., across a fault plane) and the double couple body forces that exist on either side of the dislocation surface (Burridge and Knopoff, 1964). Over time, theoretical models increased in sophistication to allow seismic energy radiation over a finite region on a fault plane (kinematic, finite-source models; Ben Menahem, 1961, 1962; Haskell, 1964). While the finiteness of rupture was represented, several assumptions had to be made about the source such as rupture area and geometry (i.e., rectangular, circular), slip history, or a constant rupture-speed. Such simplified assumptions about the source are still common in static stress drop analysis (Madariaga and Ruiz, 2016). Modern kinematic rupture models now use non-planar fault geometry and variable slip and rupture-speed; these are routine in finite-fault inversions to rapidly produce first-order details of an earthquake (Ji et al., 2002).

A major breakthrough in earthquake source modeling was in specifying the stresses (normal and shear) along the fault together with a friction model, fully describing how the fault stresses and strengths evolved with time and slip (e.g., Kostrov, 1964, 1975; Madariaga, 1976; Andrews, 1976a, b). On-fault stress and frictional strength distinguish dynamic from static and kinematic rupture models - the outcome of the earthquake is not predetermined and the boundary conditions on the fault give rise to a highly nonlinear physics problem, even when fault geometry or stress and strength distributions are relatively simple (Figure 1**)**. There are different types of dynamic rupture models, as well: quasi-dynamic rupture models prescribe stress and frictional conditions on the fault, but approximate wave propagation by ignoring inertia and using a damping term in the equation of motion, (e.g., Rice, 1993; Thomas et al., 2014) whereas fully dynamic rupture models can generate the whole wavefield by including inertia (e.g., Day, 1982). Seismic waves (body and surface waves) can promote local weakening of the fault and modify the rupture speed. Fully dynamic rupture models may simulate a single earthquake (hereafter referred to as dynamic rupture models) or multiple sequences of earthquakes (hereafter referred to as fully dynamic earthquake cycle models). Given the myriad approaches and assumptions inherent to dynamic earthquake modeling, some guidance is needed to clarify differences and highlight commonalities between approaches.

This article is timely because over the last decade, significant advances in computational hardware and software have made the field of dynamic earthquake rupture modeling flourish. But in order to effectively use these numerical tools, a *focused* understanding of the essential physics and methodologies that underpins them must be procured. Furthermore, because rupture modeling adopts techniques from several fields (i.e., fracture mechanics, seismology, computer science, applied math), it can seem overwhelming for students who are starting out to select, compile and become proficient in a specific code *in addition to* addressing their research questions in earthquake science. We build off the seminal work of Andrews (1976a, b), Day (1982), Madariaga and Olsen (2002), and others, who introduced generations of researchers to dynamic rupture models. We hope to centralize information scattered across multiple texts (e.g., Freund, 1990; Aki and Richards, 2002; Udías, Madariaga and Buforn, 2014; Igel, 2017) and link together the most essential concepts every dynamic rupture modeler should be aware of. We include in this guide a nomenclature of common terms used in dynamic rupture models (Table 1), an abridged set of scientific problems dynamic rupture models are poised to address now, as well as an example problem to illustrate the rupture model design principles we present.

2. Dynamic Rupture Model Design

What do you want to use your dynamic rupture model for?

Dynamic rupture models are excellent tools to explore potential source conditions (e.g., fault friction, stress or geometrical complexity) that contribute to seismic, geodetic or geologic observations (e.g., acceleration spectra, off-fault deformation and slip patterns). Or, in the absence of observations, these models can be used to generate a suite of scenarios to test hypotheses that govern key rupture features (e.g., rupture speed, rupture extent and surface deformation). The latter application of dynamic rupture models is referred to as a parameter study. Both approaches can leverage experimental and geologic results to inform model initial and boundary conditions such as fault zone structure or friction coefficients (Figure 1) that can be modelled in 1-D, 2-D, or 3-D. But no matter the application, it is crucial to consider the dimensionality of your simulation, which numerical methods are best suited for the problem of interest, and what observational and/or laboratory constraints on dynamic rupture parameters are available. We will discuss these aspects in the upcoming sections.

2.1 Establishing the Dimensions of the Problem

Dynamic rupture models adopt conventions from fracture mechanics for a specific type of crack mode. 2-D dynamic rupture models consider mode II (in-plane rupture) or mode III (anti-plane rupture) fault geometries that are well suited to study simple strike-slip or dip-slip fault configurations in parameter studies (Figure 2**)**. In mode II rupture, there are two degrees of

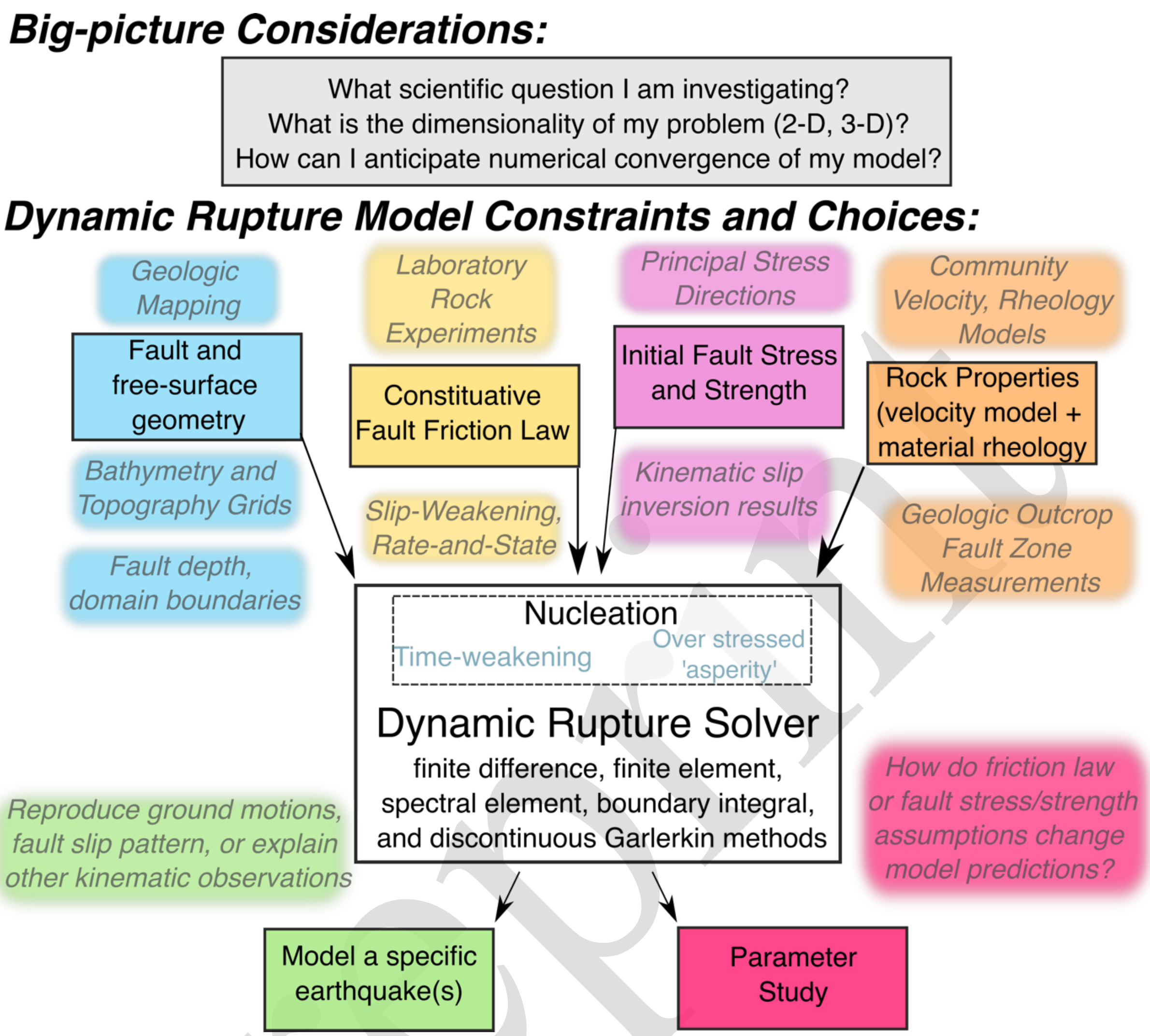

Figure 1. Generalized flowchart of how fully dynamic rupture models are constructed. We highlight two steps in model design: scientific problem formulation and dataset constraints/model choices. Color-coded words and phrases located outside of boxes are particularly important model input or outputs.

freedom that lead to SV and P wave generation whereas mode III rupture can only generate SH waves in homogeneous media. The mode I fracture represents a tensile crack and while not typically investigated with dynamic rupture models, point source models can account for fault-normal opening by separating the earthquake moment tensor into dilatational, double-couple and compensated linear vector dipole components (Knopoff and Randall, 1970). Experimental data show fault opening is possible when the fault becomes dynamically unclamped near the free-surface which indicates this mechanism can occur during earthquake slip (Anooshehpoor and Brune, 1994; Gabuchian et al., 2017; Figure 2).

3-D dynamic rupture models account for both along-strike and along-dip rupture propagation (mode II and III; Figure 2). Given the higher level of difficulty in simulation set-up and the increased number of degrees of freedom, 3-D simulations are sometimes not the first choice to run parameter studies, exceptions being for simple fault and free-surface geometries (e.g., Day, 1982; Harris and Day, 1999; Lapusta et al., 2000; Harris et al., 2002) or codes with highly optimized, parallel architectures (e.g., *FD3D_TSN*, Premus et al., 2020). 3-D dynamic rupture simulations can be particularly useful tools to incorporate variable fault and rock property conditions (Harris et al., 2021) and to reproduce ground motions of well-recorded earthquakes (e.g., 1992 Landers Earthquake, Wollherr et al., 2019; 2019 Ridgecrest Earthquake Sequence, Lozos and Harris, 2020; Zhang et al., 2020).

2.2 Choosing a Numerical Method and Setting Boundary Conditions

Dynamic rupture problems can involve heterogeneities at all scales, rendering a closed-form and analytical solution impossible in almost all cases. To solve the nonlinear boundary conditions on the fault coupled to elastodynamic wave propagation, advanced numerical techniques are required. We mention an abridged subset of dynamic rupture codes that implement the finite difference (*AWP-ODC*; Roten et al., 2016), finite element (*FaultMod*; Barall, 2009), spectral element (*SEM2DPACK*; Ampuero, 2009) or discontinuous Galerkin (*SeisSol*; De La Puente et al., 2009) methods. Madariaga and Olsen (2002) and Day et al., (2005) extensively discussed the boundary integral element and finite difference methods. Dynamic cycle models tend to incorporate the boundary element (*FDRA;* Segall and Bradley, 2012) or finite difference (*FDCycle*; Erickson and Dunham, 2014) methods. There are also recently developed hybrid models for dynamic and cycle frameworks, which combine finite element and spectral boundary integral methods in 2-D (Ma et al., 2019) and 3-D (Albertini et al., 2021). We refer the reader to Table 1 in Harris et al. (2018) and Table 2 in Erickson et al. (2020) for a more comprehensive list of fully dynamic earthquake rupture and earthquake cycle codes, respectively. A suite of numerical benchmarks was conducted by the Southern California Earthquake Center (SCEC) that compare and verify the performance of many codes on simple to complex on-fault conditions (Harris et al., 2009; 2011; 2018; Erickson et al., 2020). For in-depth introduction to some numerical techniques in the above studies, see Igel (2017).

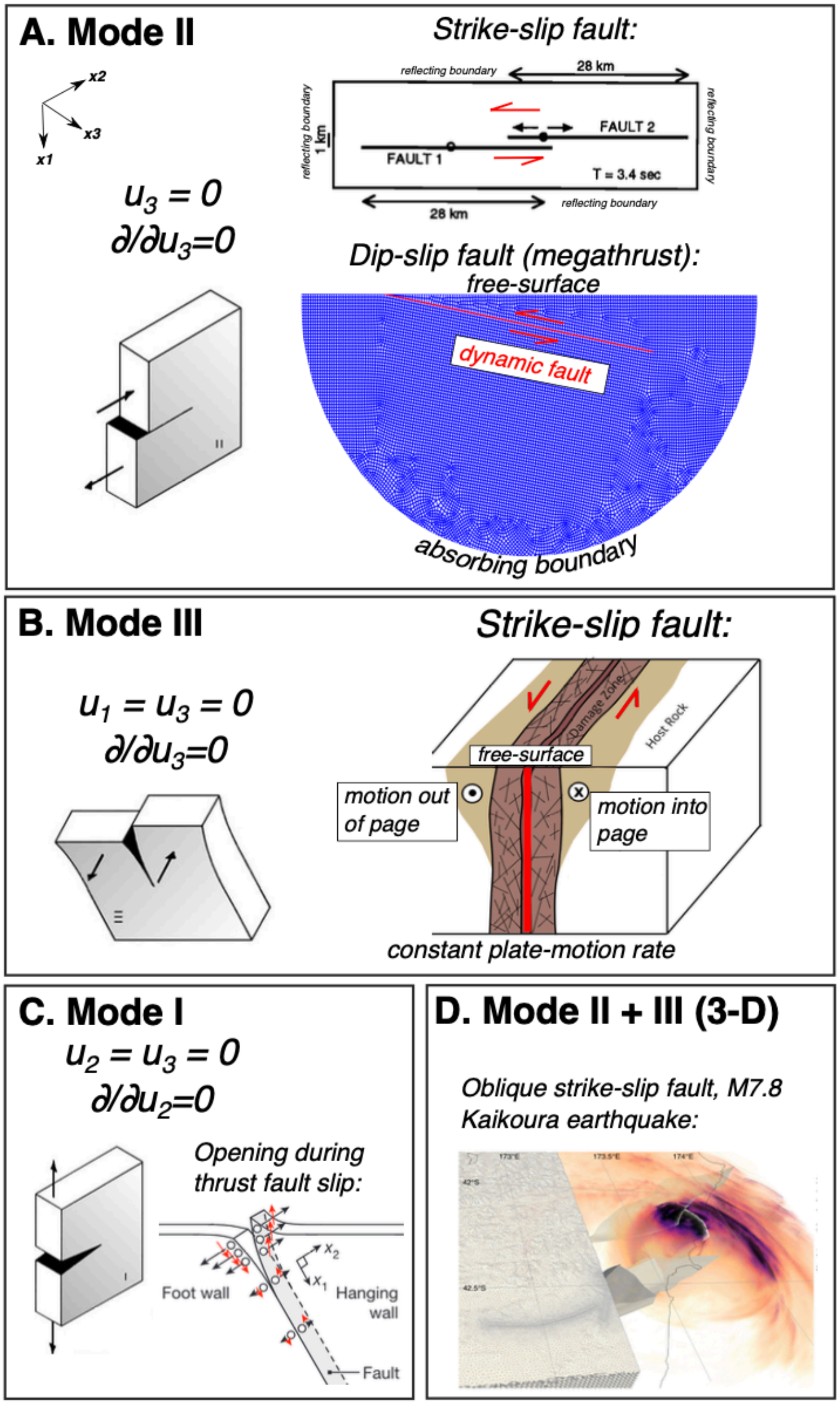

Figure 2. Rupture model geometries with examples. A) Mode II component of rupture. B) Mode III component of rupture. C) Mode I and D) 3-D dynamic rupture model that includes a mixture of mode II and III. Examples of rupture model geometries and finite element meshes are adapted from the following sources: Harris and Day (1993), Ramos and Huang (2019), Gabuchian et al. (2017), Ulrich et al. (2019). and Thakur et al (2020). Bold red lines signify the dynamic fault boundary.

The numerical method and mesh element shape can place limitations on the dynamic rupture problem of interest. Certain methods, such as finite-difference or pseudospectral methods, use the so-called "strong-form" of the set of partial differential equations. On the other hand, methods such as the finite-element, spectral-element, or variations of them involving discontinuous Galerkin methods, use the "weak-form", or the integral form of the differential equation. Although both can be proven to be mathematically equivalent, one of the major advantages of using the "weak-form" is that it implicitly accommodates the natural/Neumann boundary conditions (traction-free boundary at the earth's free surface in this case), therefore only requiring the additional Dirichlet boundary conditions to be implemented (e.g., fixed displacement at a remote boundary). Additionally, it requires a "weaker" continuity of the displacement variable (i.e., a lower order derivative on the displacement variable), making it easier to accommodate more complicated meshes. The choice of meshing can have important implications for the trade-offs between numerical complexity of solving the differential equation and incorporation of more-realistic features in a model. Certain finite-difference or pseudo-spectral methods can only handle planar fault geometries (the fault plane has a constant dip) because the meshing options are limited when using the strong-form of the differential equation (e.g., Dalguer and Day, 2007). In other cases, one may want to assess how realistic topography impacts strong ground-motion, which is a challenge for finite difference methods because of the traction-free boundary condition that must be honored at the Earth’s free surface. Finite (and high order) element methods are well suited for calculations that involve topography because when the wave equation is cast in its weak-form, the traction-free boundary requirement is implicitly satisfied (Durran, 1999).

We note that most dynamic rupture models do not incorporate the gravitational response of the material volume during coseismic rupture, and this means the model-predicted free-surface deformation field is calculated according to a mathematical formalism introduced by Okada (1985). However, there is exciting progress in coupling the response of gravity to both dynamic rupture and tsunami excitation for 2-D and 3-D problems (Lotto and Dunham, 2015; Krenz et al., 2021; Wilson and Ma, 2021).

On-fault Boundary and Initial Conditions

As mentioned earlier, one of the greatest strengths of dynamic simulations is its ability to couple frictional material failure to elastic wave propagation. The on-fault boundary conditions involve relating traction (or stress projected onto the fault surface), displacement and friction across a discontinuous fault boundary through time (Olsen and Madariaga, 2002). In many cases, there are high frequencies excited near the fault boundary that cannot be resolved by even small mesh elements and these map to numerical artifacts. Assigning a small layer of Kelvin-Voigt elements at which elastic strain can be recast to depend on a viscosity timescale, is one way to damp these high frequencies (Day and Ely, 2002). Additionally, rupture propagation involves a complex wavefield near the rupture front that must be resolved with relatively small elements adjacent to the fault, not just at the fault surface (e.g., Barall, 2009). Typical initial conditions on the fault include slip-rate and displacement being set equal to zero. Initial fault stress, strength and friction values at every mesh element are also chosen accordingly (see sections 2.4, 2.5).

Off-fault Boundary Conditions

Boundary conditions outside of the fault include absorbing and reflecting conditions. Absorbing boundaries permit elastic waves to become diminished as they encounter a particular region of the model domain. They may be implemented as perfectly matched layers (Komatitsch and Tromp, 2003) which effectively nullifies all reflection coefficients for incoming waves at any angle of incidence, or as a vanishing flux condition that permits waves to leave the model domain without reflection (Käser and Dumbser, 2006). In addition to the absorbing boundary condition, mesh coarsening towards the boundary itself (increasing mesh element size) is often implemented in order to attenuate higher wave frequencies as they pass through the larger elements.

A reflecting boundary condition is especially important to guarantee in models that include the Earth's free-surface. Some energy from seismic waves propagating from the source are reflected at the free-surface because air particles cannot exert shear stresses back onto the domain: this is physically satisfied by setting these stresses equal to zero. Also, the very existence of seismic surface waves (i.e., Rayleigh) is due to a traction-free region at the surface. The atmosphere does exert a small normal stress back onto Earth's surface as well, and this can become significant due to the overburden of the water column in the ocean. To implement this condition numerically, finite difference methods have relied on stress imaging or vacuum formalism approaches, which prescribe antisymmetric stress tensor components or zero elastic moduli above the free surface, respectively (Moczo et al., 2014). On the other hand, finite element and spectral element methods implicitly satisfy the traction-free condition because when the integral of the spatial part of the wave equation is taken at the domain boundaries, the resultant integration limits at the free-surface are set to zero. A well-known method to verify reflecting boundary conditions is to numerically solve Lamb's problem (Lamb, 1904), which has an analytical solution to compare to. Lamb's problem consists of a vertical force excitation at the free-surface recorded at a synthetic seismogram receiver some distance away from the source in a homogeneous, isotropic and linearly elastic half-space.

2.3 Ensuring Numerical Convergence

If a heterogeneous velocity model is used, the lowest shear-wave speed (and corresponding smallest wavelength) will typically determine the maximum element mesh size required to resolve that wavelength. The element mesh size (and shape) can also impact the details of the constitutive fault friction law (see section 2.4), the fault and free-surface geometries, and how the earthquake is allowed to start (nucleation, see section 2.6). To generate realistic free-surface geometries from topography or bathymetry datasets using finite elements, knowledge of advanced meshing software is required. Open-source or commercially available meshing software include Gmsh (Geuzaine and Remacle, 2009), Cubit (Coreform Cubit), or Simetrix (*SIMetrix* ref manual). But mesh design can be a laborious process and is dependent on the specific numerical method employed in the rupture modeling code. In fact, building a high-quality mesh can often take as much - if not more - time than running a parameter space study. It is encouraged to build simpler examples before incorporating non-planar fault and free-surface geometries from scratch.

A key parameter that must be resolved during dynamic rupture propagation is the cohesive zone width (Λ, Day et al., 2005). The cohesive zone is the region behind the rupture-front where fault strengths decrease from their static to dynamic level. Λ represents a fundamental length scale in dynamic rupture problems where slip-rate and stress can vary significantly; it may be visualized or measured from a plot of slip-rate as a function of position on the fault at a particular time-step. Depending on the type of friction law used, we can analytically derive an estimate for the size of this cohesive zone using energy balance and linear stability analysis from dynamic fracture mechanics (Rubin and Ampuero, 2005; Ampuero and Rubin, 2008). Equation 1 below gives the general form of the cohesive zone width at zero speed (initiation of rupture) when using a linear slip-weakening friction law (Day et al., 2005),

$$\Lambda = \frac{C_1}{C_2}\left[\frac{G D_c}{\Delta\sigma_d}\right]^2 \left[\frac{1}{1+\frac{L_0^2}{L^2}}\right]^{-1} \tag{1}$$

where the C_i terms are constants, G is the shear modulus, D_c is the critical slip distance, $\Delta\sigma_d$ is the dynamic stress-drop and L_o is the critical half-crack length (a necessary length for nucleation of mode II or mode III cracks from energy balance considerations); see Nomenclature Table for definitions of D_c and $\Delta\sigma_d$. In general, Λ shrinks as rupture-front speed accelerates away from where the earthquake is nucleated because it undergoes Lorentz contraction. It is recommended that in the presence of other heterogeneous properties, one should strive to resolve the *median* cohesive zone width (see sections 6 in Day et al., 2005 or section 4.2 Wollherr et al., 2018). The minimum number of points in a mesh element needed to span Λ for a well-resolved dynamic rupture model changes according to numerical method and medium properties, and resolving the cohesive zone based on these theoretical estimates may not be optimal for more complicated problems. For instance, if spontaneous dynamic rupture is modelled with a second-order finite difference or boundary integral method within a homogeneous and linearly elastic medium, then only five points are required (Day et al., 2005). If an Arbitrary high-order Derivative-Discontinuous Galerkin (with sub-element point resolution) is used with heterogeneous stress, then as few as one to two points are needed if a high polynomial order ($\geq$ 6) is used for the orthogonal basis functions which interpolate solutions between discrete elements (Wollherr et al., 2018).

One method to ensure that a dynamic rupture simulation converges well is to run simulations with decreasing on-fault mesh element size and compare, for example, the root-mean-square difference of rupture-time arrival as a function of element size (e.g., Appendix A of Huang and Ampuero, 2011). Kinematic features of the rupture (e.g., final slip, surface deformation, and slip-rate) can be generally compared for meshes of decreasing element sizes as a function of time or space to assess how solution sensitivity varies. We also note that one should run a simulation long enough for seismic waves to reach the absorbing boundaries of the model domain such that the dynamic wavefield is no longer interacting with the fault.

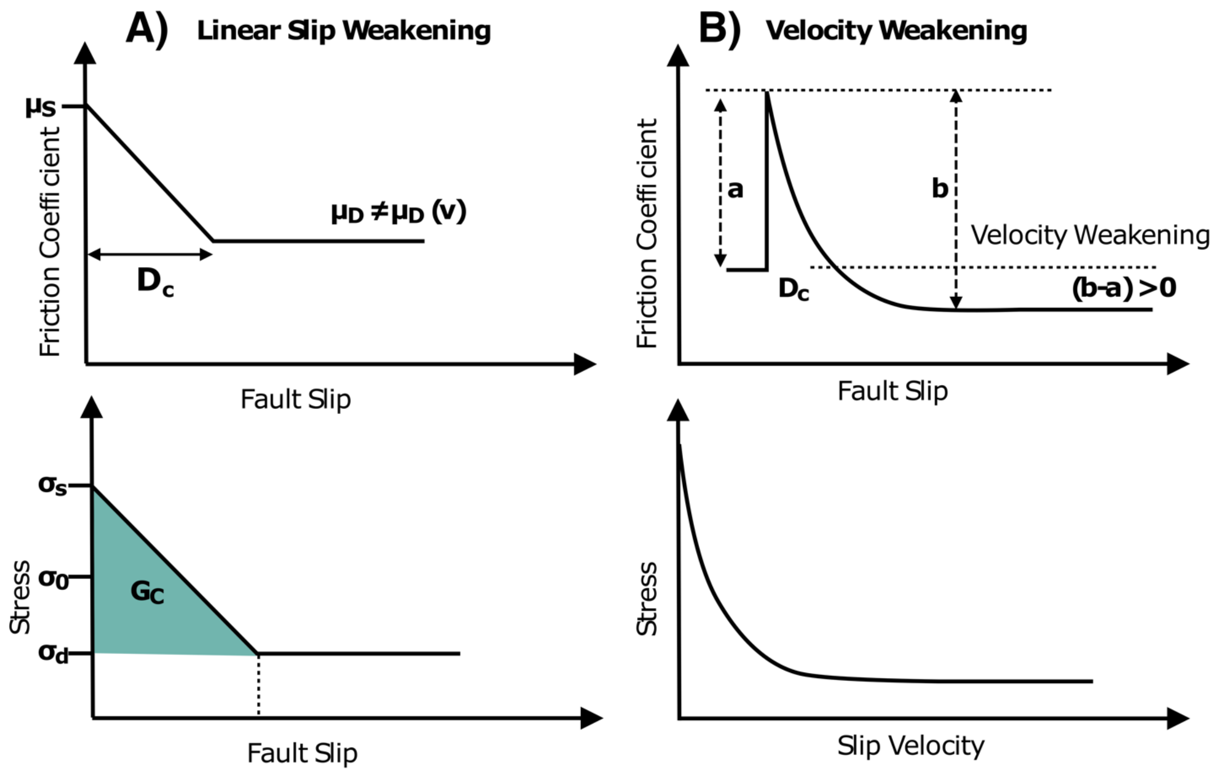

Figure 3. A comparison between the A) linear slip-weakening and B) velocity-weakening friction laws used in dynamic rupture models. The top row shows how the friction coefficient evolves during rapid sliding in an earthquake, pictorially relating the parameters in equations 2 and 3. The bottom row shows the explicit dependence of stress on slip or slip-velocity. The shaded region (G_c) denotes the fracture energy. These plots are inspired by figures appearing in Marone and Saffer (2007) and Zhang et al., (2003).

*2.4 **Choice of friction law - how slip locally evolves on the fault through time***

Frictional strength keeps two sides of rock along a fault in place before an earthquake happens. During dynamic rupture, friction can depend on myriad of factors, the most important are thought to be slip, slip-rate, and contact time (Duab and Carlson, 2010). Two common friction laws used in modeling coseismic rupture include the slip-weakening and velocity-weakening formulations.

In the slip-weakening friction law, the dynamic friction coefficient (μ_d) only depends on slip and is characterized by the slip-weakening critical distance (D_c), which also controls the amount of fracture energy available to grow the earthquake (Ida, 1972; Palmer and Rice, 1973, Andrews, 1976b).

$$\mu = \begin{cases} \mu_s - (\mu_s - \mu_d) \cdot \frac{D}{D_c}, & D \leq D_c \\ \mu_d, & D > D_c \end{cases} \qquad (2)$$

Expression 2 describes this friction law where D is the local fault slip and μ_s is the static friction coefficient. In the slip-weakening framework, the relative difference between μ_d and μ_s determines if the earthquake has the necessary energy to propagate (Figure 3a). Specifically, if $\mu_d < \mu_s$, there is a finite drop in fault strength and this behavior is called slip-weakening; if $\mu_d = \mu_s$, there is no energy to grow the propagating shear crack; finally, if $\mu_d > \mu_s$, then there is a deficit in the available work to advance rupture which is termed slip-strengthening. The last case can be used to arrest rupture or to roughly mimic velocity-strengthening behavior (see following discussion). It therefore makes physical sense for earthquakes to nucleate (section 2.7) within the 'weakening' frictional regions of the fault.

Fracture energy is the energy that must be overcome on the fault to grow the propagating shear crack and can be calculated as half the product of the strength drop (section 2.6) and Dc in the linear slip-weakening friction law (Figure 3a; Table 1). Typical values of D_c range from 0.1 to 2 m. The influence of increasing D_c is to increase the fracture energy and thus decrease the rupture speed for the same stress and frictional conditions because the ratio between radiated energy to fracture energy is smaller. Because there is a strong trade-off in fault strength drop (see section 2.5) and fracture energy, D_c cannot be uniquely constrained in most cases through seismic inversion techniques (Guatteri and Spudich, 2000). But the fracture energy can be exactly calculated in dynamic rupture models (Andrews, 1976b) and sometimes be estimated with seismic recordings assuming an energy balance model for the earthquake (e.g., Abercrombie and Rice, 2005).

Velocity-weakening laws (also termed strongly velocity-weakening) capture the general observation that fault friction is inversely proportional to slip-rate during an earthquake (Cochard and Madariaga, 1994; Ampuero and Ben-Zion, 2008; Figure 3b). Velocity weakening friction laws are typically regularized by a cut-off velocity (V_c) which influences the direct and evolution effects of this friction law (a and b, respectively).

$$\mu_d = \mu_s + a\frac{V}{V + V_c} - b\frac{\theta}{\theta + V_c} \quad (3)$$

Here, V is the fault slip-rate and θ is a state variable likened to the contact duration between asperities (locked patches) on the fault. Typical ranges for a and b in expression 3 span 0.001 – 0.1 (Ampuero and Ben-Zion, 2008; Kozdon and Dunham, 2013). Similar to the slip-weakening framework, the relative difference in these parameters ($a - b$) controls when the fault exhibits velocity-weakening ($a - b < 0$), neutral ($a - b = 0$) or strengthening ($a - b > 0$) frictional behaviors. V_c can be interpreted as the speed of fault slip near the initiation of rupture and laboratory models show that it may range from 0.05 – 2 m/s (Beeler et al., 2008). The main difference between slip-weakening and velocity-weakening friction laws is that the latter allows for the fault to heal (i.e., the slip-rate behind the rupture front approaches zero in the model; Figure 3) and thus tends to generate pulse-like rupture characteristics (Heaton, 1990) whereas the slip-weakening friction law favors crack-like propagation (i.e., a non-zero slip-rate extends relatively far behind the rupture front). Note that slip-weakening friction laws can still generate pulse-like slip-rate functions if barriers exist along the fault such as increased dynamic friction, low shear stress, or additional heterogeneities like a low seismic velocity fault zone. In the limit of increasing slip-rate amplitude, θ- dependent friction laws can begin to approximate slip-weakening behavior (Cocco and Bizzarri, 2002; Okubo and Dieterich, 1984; Dieterich, 2007; Ryan and Oglesby, 2014).

There are more complex friction laws that take into account thermal weakening and pore fluid pressurization (Andrews, 2002; Noda et al., 2009) or even flash heating (Beeler et al., 2008); these can be invoked in a dynamic rupture simulation if the problem warrants this type of physics (i.e., the potential of induced seismicity near georeservoirs; Mai et al., 2021). The choice of friction law can impact simulation results in several ways including the predominance of crack-like versus pulse-like rupture propagation style (Gabriel et al., 2012) or how rupture evolves over irregular fault geometry along-strike and along-dip (Ryan and Olgesby, 2014, 2017; Luo and Duan, 2018). Sometimes, one friction law is preferred over another because simpler models can fit the observations satisfactorily and do not require multiple (and unconstrained) Earth parameters.

2.5 Establishing constraints on fault strength and stress

The normal stress and frictional coefficients (static and dynamic) set the relative fault strengths. The effect of pore pressure in the earth is often folded into the normal stress by subtracting a gradient from the depth-dependent lithostatic stress, termed the effective normal stress. Effective normal stress can be constrained from information about the greatest and least principal stresses (e.g., Aochi and Fukuyama, 2002) or by assuming a constant pore pressure gradient (e.g., 27 MPa/km; Rice, 1992; Suppe, 1985). Many dynamic rupture models set the effective normal stress equal to a constant amplitude of ~50 MPa at seismogenic depths of interest (~5 km < z < 20 km), which is born from the high pore pressure assumption present in mature fault zones (Rice, 1992). μ_s is typically assumed to be near 0.6, to be consistent with Byerlee's law (Byerlee, 1978) and $\mu_d$is sometimes inferred from lab experiments that shear rock at slip rates comparable to coseismic values (e.g., Di Toro et al., 2011), or from dynamic friction levels obtained for rocks collected at or near Earth's surface (e.g., Harris et al., (2021), who used information from Morrow et al. (2010) and Moore et al. (2016)). The product of effective normal stress and μ_s is termed the static fault strength and the product of effective normal stress and μ_d is termed the dynamic fault strength (Table 1).

Initial shear stress is one of the more difficult parameters to estimate in a dynamic rupture model. But its amplitude is crucial in determining the dynamic stress-drop ($\Delta\sigma_d$), which is defined as the shear stress minus the dynamic fault strength - this parameter essentially gives how much total energy is available to consume on the fault, influencing how large the modeled earthquake may become. Strategies for setting the initial shear stress on faults can include assuming a constant regional stress field, then projecting this field onto a fault of variable strike, leading to a heterogeneous distribution (e.g., Pelties et al., 2012). If the azimuth of maximum horizontal compressive stress, principal stress components, orientation of the intermediate principal stress field, and seismogenic depth can be constrained, then the relative prestress ratio can be estimated (e.g., Methods section in Ulrich et al., 2019). Other methods use fault slip distributions derived from kinematic inversion (e.g., Olsen et al., 1997; Ripperger and Mai, 2004) or slip deficit estimated from geodetic methods (e.g., Hok et al., 2011; Yang et al., 2019; Ramos et al., 2021) to constrain initial shear stress. If kinematic slip distributions are used to constrain shear stress, the expected stress change from the imposed slip is first calculated and then added to dynamic fault strength - this reflects complete stress drop from the last earthquake and assumes stress accumulates approximately linearly during the interseismic period (e.g., Yang et al., 2019; Ramos et al., 2021). An alternative approach considers nonlinear stress accumulation between large earthquakes through coupling of long-term geodynamic models to dynamic rupture models, setting the initial stress conditions informed by multiple tectonic cycles (van Zelst et al., 2019). Such coupled models are now being used for physics-based tsunami hazard assessment (e.g., Madden et al., 2020; Aniko Wirp et al., 2021). And still others have prescribed stochastic shear stress distributions on faults to capture variability in the true state of tectonic loading on a fault (Oglesby et al., 2002; Guatteri et al., 2003; Andrews and Ma, 2016), some with an aim to produce higher frequency (≥1 Hz) ground motions. Another interesting perspective to constrain the nature of stress release is through dynamic rupture inversion. These types of models seek to untangle the coupling of fault stress/strength and friction law parameters through nonlinear (Bayesian) inversion and while difficult, have shown promise to estimate the stress drop, static fault strength, and friction drop in subduction zone (Herrera et al., 2017) or intra-continental (Gallovič et al., 2019, 2020) tectonic environments.

It is well known that natural faults are not planar objects with uniform dip – they have micro to macro-scale complexities (10^{-9} – 10^{3} m) that can be described as self-similar fractals (Anderson, 1951; Power and Tullis, 1991; Candela et al., 2012). This nonplanarity can be described as 'roughness' in dynamic rupture models and is prescribed in two general ways: 1) extreme heterogeneity in the normal and shear stress amplitudes that is expected from a non-planar fault surface, or 2) by explicitly modeling geometrical complexity into the finite element mesh surface representing the fault plane. 2-D dynamic rupture models demonstrated that a root-mean-square stress perturbation (of the shear or normal stress amplitudes) that is inversely proportional to the smallest spatial wavelength can generate acceleration spectra that are consistent with ground motion models (Dunham et al., 2011; Fang and Dunham, 2013 and mathematical details therein). Geometrical fault roughness may lead to bursts of supershear rupture (see section 2.7) that are not observed on geometrically planar fault models (i.e., Bruhat et al., 2016). Accounting for the influence of roughness may add a dimension of geologic realness to a simulation because numerous field and experimental analyses show how fault plane geometry affects stress (e.g., Brodsky et al., 2020), and the finiteness of fault zones in general (e.g., Rowe et al., 2013). We note that roughness in dynamic rupture models is computationally demanding – a way to ameliorate this is to capture the statistically relevant features of roughness and use kinematic rupture models that are informed by the dynamic ones (e.g., Savran and Olsen, 2020).

2.6 Nucleation - making your earthquake go

How does an earthquake start? Geophysical studies of the nucleation process suggest two conceptual models: large earthquakes can be triggered by random interactions of stress release from smaller earthquakes *or* a gradual, deterministic build-up of stress driven by transient slow-slip (Gomberg, 2018). In dynamic models, the nucleation process has justification from fracture mechanics (specifically, the balance between energy release rate and fracture energy that determines a critical instability length), but is otherwise a numerical parlor trick. The goal is to guard against overly harsh nucleation (i.e., excessive imposed shear stress, critical fracture length, or rupture velocity) as this will contaminate the rest of the modeled earthquake and bias results (Galis et al., 2015).

There are two general nucleation approaches for dynamic rupture models: the time-weakening (TW; Andrews, 1985) or overstressed patch (Kanamori, 1981) method. Both approaches recognize a finite length scale where the earthquake may start with a specified shear stress level. In TW, an imposed rupture velocity is prescribed over a short time scale at a critical half-crack length (2-D dynamic problems; Andrews, 1976) or a critical radius (3-D dynamic rupture problems; Day, 1982). The critical length scale is inversely proportional to the dynamic stress drop for both TW variations. This makes intuitive sense as larger dynamic stress drop means a higher amount of initial shear stress. The imposed rupture velocity is typically chosen to be ~75% of the Rayleigh wave speed (Bizzarri, 2010). The overstressed patch differs in the respect that it does not prescribe a temporal component or imposed rupture velocity: the initial shear stress is made to be slightly above the static fault strength (~0.5% of the strength; Galis et al., 2015), meaning that the fault fails instantaneously at the start of the simulation. This perspective draws from the asperity model of earthquakes where a localized, high stress instability is enough to cause wholesale failure of the fault. For ruptures using a slip-weakening friction law, parameter studies have rigorously explored and contrasted the relationships between stress level and asperity area in 2-D and 3-D geometries (Galis et al., 2015 and references therein).

Once nucleation ceases, the competition between relative fault stresses/strengths and friction law ultimately control how the earthquake evolves. On that note, an important parameter to consider (even before running a simulation) is the S-ratio, defined as S = $(\sigma_s - \sigma_o) / \Delta\sigma_d$ (Andrews, 1976b; Das and Aki, 1977) where σ_s is the static fault strength and σ_o is the initial shear stress. If S $<$ 1.77 (in 2-D homogeneous, linearly elastic media) or S < 1.19 (in 3-D media) a special rupture speed termed supershear can occur, which is an emergent rupture-front that travels above the S-wave velocity (Andrews, 1985; Dunham, 2007). This feature was first inferred from the 1979 M6.6 Imperial Valley earthquake (Archuleta, 1984). Most observations of earthquake rupture speed suggest faults unzip at sub-Rayleigh velocities, making supershear ruptures unique and responsible for stronger, pulse-like ground motions close to the fault. Supershear is less observed for dip-slip faults (e.g., subduction zone megathrusts), but has been observed at strike-slip faults under some conditions (Bouchon and Vallée, 2003; Weng and Ampuero, 2020).

2.7 Rock Material Properties (velocity models and rheology)

The structure of Earth's lithosphere is heterogeneous across all measured spatial scales. Plate tectonics and surface processes have generated a plethora of rock lithologies that have different elastic moduli, setting the speed limits of seismic body and surface waves. There are a few 3-D velocity models of the rock properties that can be used in dynamic rupture models (SCEC Community Velocity Model, Small et al., 2017; Cascadia Velocity Model Stephenson et al., 2017), but unfortunately, such detailed knowledge is generally unavailable near major faults in less economically advantaged countries (despite a clear seismic risk). Why should you consider the rock properties surrounding a fault? If you have accurate information on seismic wave speeds, then dynamic models can be used to generate synthetic recordings of strong ground shaking or to probe specific path and source effects that could contribute to observations. Even in 2-D dynamic rupture problems that incorporate a 1-D velocity structure, both shallow and deep rock properties can play a role in the frequency content of earthquake rupture (Huang, 2021; Yin and Denolle, 2021). On the other hand, assuming a homogeneous velocity structure is advantageous if you want to assess the role of other parameters like topography on your dynamic rupture problem (e.g., Kyriakopoulos et al., 2021).

Besides the velocity structure, choosing a non-elastic rheology of the host rock can dramatically influence dynamic wavefield interactions and change the earthquake characteristics. Dynamic rupture models that invoke a plastic material behavior immediately outside the fault zone (off-fault) can explain the pattern of slip at shallow depths (Roten et al., 2017), generate plastic strain distributions that are consistent with geologic field observations including flower structures (Ma and Andrews, 2010), and modify the stress levels and nucleation sizes needed to sustain a particular rupture propagation behavior (Gabriel et al., 2013). Some general implications of off-fault plasticity for numerical mesh resolution are a wider Λ and lower rupture speed (Andrews, 2005; Wollherr et al., 2018, and others), the former of which means fewer fault elements are required to resolve Λ compared to purely elastic rheologies. There is also work assessing the role of fault damage zones that can exist in mature fault systems (e.g., the San Andreas fault zone). Fault damage zones are numerically represented in dynamic rupture models as regions characterized by a lower shear modulus (e.g., Harris and Day, 1997; Huang et al., 2011, 2014; Huang, 2018; Thakur et al., 2020). Inclusion of these features in simulations has begun to tie together how mature vs. immature faults can drive differences in the earthquake recurrence interval, which is a key parameter estimated from paleoseismic analyses (Wallace, 1970).

3. Example Dynamic Earthquake Rupture Problem

In this section, we walk through SCEC benchmark problem TPV_16 (https://strike.scec.org/cvws/cgi-bin/cvws.cgi) (Harris et al., 2018) to illustrate key principles of physics-based rupture simulation setups. Multiple numerical methods have been used on this benchmark problem, thus ensuring solution reproducibility and robustness. We choose to show the numerical results produced by the staggered-grid finite-difference method of AWP-ODC (Olsen, 1994) for simplicity. The 3-D fault geometry of TPV_16 represents a vertical strike-slip fault (90 ° dip) that is 19.5 km deep and 48 km long with a node spacing (Δh) of 75 m in the x, y and z directions (Figure 4a). The medium is homogeneous, isotropic and linearly elastic defined by a density of 2670 kg/m^3, and p and s-wave speeds of 6000 and 3664 m/s, respectively.

Absorbing boundary conditions (perfectly matched layers) are applied to the model on all sides except the free-surface, which is a reflecting boundary. This particular simulation is run for a total of 15 seconds.

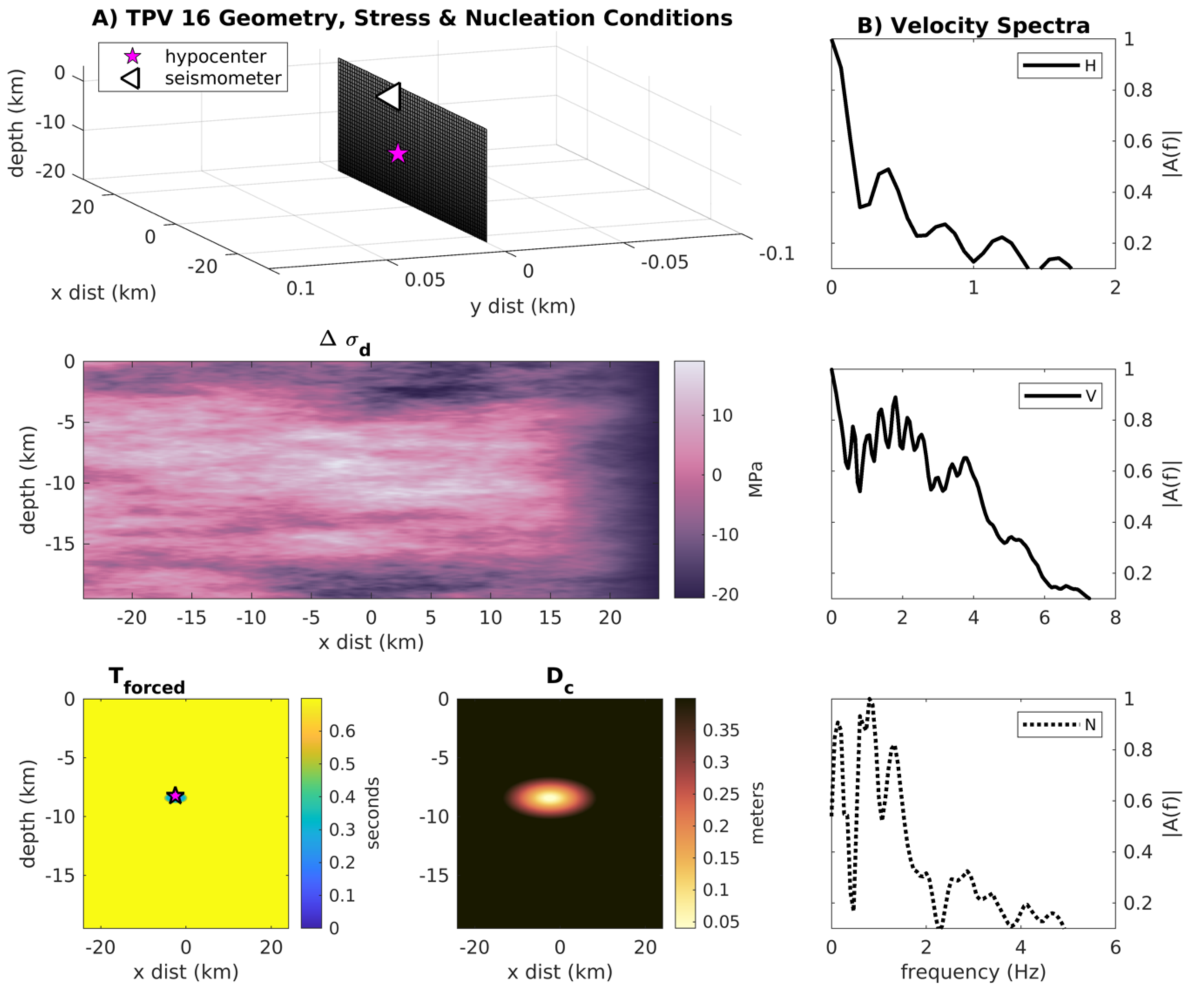

Figure 4. Example dynamic rupture model problem from the SCEC benchmark exercise TPV 16 (Harris et al. 2018). A) On-fault geometry (planar right-lateral strike-slip fault), initial dynamic stress drop ($\Delta\sigma_d$) distribution, forced rupture time (T_{forced}) and critical slip-weakening distance (D_c). The latter two parameters are required for nucleation. B) Representative off-fault seismogram spectra (normalized) of the horizontal (H), vertical (V) and normal (N) velocity time series for the seismic station shown in A. Note the different x-axis limits for the frequency content.

The fault friction law is linear slip-weakening with the following parameters specified at every point on the fault: D_c, μ_s, μ_d , C, and T. C is the rock cohesion, a part of the fault strength (i.e., σ = C + $\mu\sigma_n$). T is the time weakening value that controls forced rupture ($T_{forced,}$ Figure 4a) - outside the nucleation region, it is equal to a very large value (i.e., 1.0 x 10^9). For this particular example, nucleation is a two-stage process of forced rupture at ~8 km depth (Figure 4a). The first stage consists of increasing T_{forced} from zero seconds to a time that ensures the rupture speed to be sub-Rayleigh (35% of the shear-wave speed). The second stage gradually increases D_c from 0.04 m to 4 m in two separate radial zones, effectively increasing the fracture energy such that spontaneous rupture is sustained at a sub-Rayleigh rupture speed after the time-weakening procedure ends.

The initial normal stress is set to a constant level of 60 MPa on the fault whereas the initial shear stress is generated from a Boltzmann distribution that relies on concepts from thermodynamics and statistical mechanics (Figure 4a; Barall and Harris, 2012). Randomized stress fields can be useful proxies for the heterogeneous conditions operating on real faults (due to fault surface heterogeneity or earthquake stress release) and moreover, explain some observations of variable peak slip-rate and rupture velocity quite well (Day, 1982). This particular initial shear stress field leads to a highly variable dynamic stress drop, which ultimately controls the spatial extent of rupture (Figure 4a).

To ensure that the cohesive zone Λ is resolved during dynamic rupture, we calculate the zero-rupture-speed Λ (Λ_o) as an upper bound for both mode II and III directions (expression 30a in Day et al., 2005). Using the given frictional parameters and medium properties (i.e., D_c, μ_d, μ_s, σ_n, and the shear modulus), Λ_o can either be 926.1 m or 694.5 m (for mode II and mode III, respectively). The ratio of Λ_o to the node spacing ($N_c = \Lambda_o/\Delta h$) should be at least five for finite difference methods (Day et al, 2005). Our calculations suggest that N_c is approximately 9 – 12 for mode II and mode III Λ_o, which insures a well resolved Λ_o and numerically stable simulation.

We also assess the frequency content of the recorded waveforms at the free-surface (Figure 4b). Each seismogram has a sample rate of 125 samples/second, which leads to a Nyquist frequency of ~63 Hz. A dominant frequency appears to be ~2 Hz on the vertical component (Figure 4b), which suggests the shortest resolvable wavelength is approximately 1.8 km (for the given shear-wave speed) and at least 24 Δh are sampling this wavelength. Of course, the frequency content between the three wavefield components is variable in Figure 4b, which is probably controlled by the stochastic nature of the on-fault stress drop.

4. Conclusions and Outlook

Dynamic rupture and fully dynamic cycle models are useful tools to test hypotheses about earthquake processes. Able to span the coseismic (10^1 seconds) to interseismic time scales (10^{10} seconds), these models are sensitive to the choice of numerical method and boundary conditions as well as the available geological/geophysical data to constrain them. The burgeoning availability of computational resources (e.g., cloud computing, GPU's and exa-scale computing) and access to open-source software makes running these simulations feasible, but practitioners still must be aware of the essential physics and techniques to ensure a well resolved, physically plausible model. This guide walked through major concepts that are common to both dynamic rupture and fully dynamic cycle models: model design (problem dimensions and purpose), numerical convergence, on-fault initial and boundary conditions (stress, strength and friction), earthquake nucleation and off-fault properties (velocity model, material behavior). We did not provide a thorough review of fully dynamic cycle models and we refer the interested reader to the recent work on numerical benchmarks from the cycle modeling community (i.e., Erickson et al., 2020; Jiang et al., 2022).

Wherever possible, we cited the latest research to foster inspiration and highlight a particular numerical method. We also stepped through an example SCEC benchmark problem to showcase the implementation of the principles we believe are key to running a successful numerical experiment. As we look into the future, we imagine the dynamic perspective of earthquakes will be continually strengthened by evolving code development, high quality observations near active faults, and collaborations between geologists, geophysicists, and computational scientists alike.

Data and Resources

No new data were used in this study. The simulation input and output data for the example dynamic rupture problem are available through the Southern California Earthquake

Center/United States Geological Survey Spontaneous Rupture Code Verification Project (https://strike.scec.org/cvws/).

Acknowledgements

M. D. R, P. T., and Y. H. acknowledge funding from the National Science Foundation EAR-1943742 grant. R. A. H. from the USGS Earthquake Hazards Program. We appreciate the constructive comments by two anonymous reviewers. We also thank USGS and AFRL internal reviewers Fred F. Pollitz and Raymond J. Willemann for their helpful suggestions on an earlier version of this manuscript. Any use of trade, firm, or product names is for descriptive purposes only and does not imply endorsement by the U.S. Government.

References

Abercrombie, R. E. and J.R. Rice (2005). Small earthquake scaling revisited: can it constrain slip weakening? *Geophys. J. Int.*162, 406–424. doi:10.1111/j.1365-246X.2005.02579.x

Albertini, G., A. E. Elbanna, and D. S. Kammer (2021). A three-dimensional hybrid finite element – spectral boundary integral method for modeling earthquakes in complex unbounded domains. *International Journal for Numerical Methods in Engineering*. doi:10.1002/nme.6816

Ampuero, J. P. (2009). SEM2DPACK: A spectral element method tool for 2D wave propagation and earthquake source dynamics, User's Guide, version 2.3.6. Retrieved from http://www.sourceforge.net/projects/sem2d

Ampuero, J.-P., and Y. Ben-Zion (2008). Cracks, pulses and macroscopic asymmetry of dynamic rupture on a bimaterial interface with velocity-weakening friction. *Geophys. J. Int*, *173(2), 674–692, doi:10.1111/j.1365-246X.2008.03736.x.*

Ampuero, J. P., and A. M. Rubin (2008). Earthquake nucleation on rate and state faults–Aging and slip laws. Journal of Geophysical Research: Solid Earth, 113(B1). doi:10.1029/2007JB005082

Anderson, E. M. (1951). The Dynamics of Faulting, 2nd ed., 206 pp., Oliver and Boyd, Edinburgh, Scotland

Andrews, D. J. (1976a). Rupture Propagation with Finite Stress in Antiplane Strain. *Journal of Geophysical Research*, *81*(20), 3575–3582. doi:10.1029/JB081i020p03575

Andrews, D. J. (1976b). Rupture velocity of plain strain shear cracks. *J. Geophys. Res.*, 81. 5679 – 5687. **doi:10.1029/JB081i032p05679**

Andrews, D. J. (1985). Dynamic plane-strain shear rupture with a slip-weakening friction law calculated by a boundary integral method. *Bull. Seismo. Soc. Am.* ,75(1), 1–21. doi:10.1785/BSSA0750010001

Andrews, D. J. (2002). A fault constitutive relation accounting for thermal pressurization of pore fluid. *Journal of Geophysical Research: Solid Earth*, *107*(B12), ESE 15-1-ESE 15-8. doi:10.1029/2002jb001942

Andrews, D. J., and S., Ma. (2016). Validating a Dynamic Earthquake Model to Produce Realistic Ground Motion, *Bull. Seismo. Soc. Am.*, 106(2), 665-672, doi:10.1785/0120150251

Anooshehpoor, A., and J. N. Brune (1994). Frictional Heat Generation and Seismic Radiation in a Foam Rubber Model of Earthquakes. In *PAGEOPH* (Vol. 142, Issue 4). doi: 10.1007/BF00876062

Aochi, H., and E. Fukuyama (2002). Three-dimensional nonplanar simulation of the 1992 Landers earthquake, *J. Geophys. Res.,* 107(B2), 2035, doi:10.1029/2000JB000061

Archuleta, R. J. (1984). A faulting model for the 1979 Imperial Valley earthquake, *J. Geophys. Res*., 89(B6), 4559-4585. doi:10.1029/JB089iB06p04559

Barall, M. (2009). A grid-doubling finite-element technique for calculating dynamic three-dimensional spontaneous rupture on an earth-quake fault, *Geophys. J. Int.*,178, no. 2, 845–859, doi:10.1111/j.1365-246X.2009.04190.x

Barall, M., and R. A. Harris (2012). Thermodynamic method for generating random stress distributions on an earthquake fault*: U.S. Geological Survey Open-File Report*. 2012–1226, 112p.

Barall, M., and R. A. Harris (2015). Metrics for comparing dynamic earthquake rupture simulations, *Seismol. Res. Lett*. 86, no. 1,223–235, doi:10.1785/0220140122

Beeler, N. M., Tullis, T. E., and Goldsby, D. L. (2008). Constitutive relationships and the physical basis of fault strength due to flash heating. *Journal of Geophysical Research,* 113, B01401, doi:10.1029/2007JB004988.

Ben-Menahem, A. (1961). Radiation of seismic surface waves from finite moving sources. *Bulletin of the Seismological Society of America*, 51, 401 - 453. doi:10.1785/BSSA0510030401

Ben-Menahem, A. (1962). Radiation of seismic body waves from finite moving sources in the Earth. *Bulletin of the Seismological Society of America*, 67, 396 - 474.

Ben-Menahem, A. (1995). A Concise History of Modern Seismology: Origins, Legacy and Perspective. *Bulletin of the Seismological Society of America*, 85, 1202- 1225. doi:10.1785/BSSA0850041202

Bizzarri, A. (2010). How to promote earthquake ruptures: Different nucleation strategies in a dynamic model with slip-weakening friction. *Bulletin of the Seismological Society of America*, *100*(3), 923–940. doi:10.1785/0120090179

Bouchon, M., and M. Vallée (2003). Observation of long supershear rupture during the magnitude 8.1 Kunlunshan earthquake. *Science.* 301, 824–826. doi: 10.1126/science.1086832

Brodsky, E. E., G. C. McLaskey, and C.-Y. Key (2020). Groove generation and coalescence on a large-scale laboratory fault. *AGU Advances,* 1, e2020AV000184. doi: 10.1029/2020AV000184

Bruhat, L., Z. Fang, and E. M. Dunham (2016). Rupture complexity and the supershear transition on rough faults. *Journal of Geophysical Research: Solid Earth*, *121*. doi:10.1002/2015JB012512

Burridge, R. and L. Knopoff (1964). Body Force equivalents for seismic dislocations. *Bull. Seism. Soc. Am.*, 54, 1875-1888. doi:10.1785/BSSA05406A1875

Candela, T., F. Renard, Y., Klinger, K., Mair, J., Schmittbuhl, and E., Brodsky (2012). Roughness of fault surfaces over nine decades of length scales. *Journal of Geophysical Research,* 117, B08409. doi:10.1029.2011JB009041.

Cocco, M., and A. Bizzarri (2002). On the slip-weakening behavior of rate- and state dependent constitutive laws. *Geophysical Research Letters*, *29*(11), 1–4. doi:10.1029/2001GL013999

Coreform Cubit (Version 2020.1) [Computer software]. Orem, UT: Coreform LLC. Retrieved from http://coreform.com

Day, S.M., and G. P. Ely (2002). Effect of a shallow weak zone on fault rupture : numerical simulation of scale-model experiments, *Bull. seism. Soc. Am.*, 92(8), 3022–3041

Day, S. M., L. A. Dalguer, N. Lapusta, and Y. Liu (2005). Comparison of finite difference and boundary integral solutions to three-dimensional spontaneous rupture. *Journal of Geophysical Research: Solid Earth*, *110*(12), 1–23. doi:10.1029/2005JB003813

de La Puente, J., J. P. Ampuero, and M. Käser (2009). Dynamic rupture modeling on unstructured meshes using a discontinuous Galerkin method. *Journal of Geophysical Research: Solid Earth*, *114*(10), 1–17. doi:10.1029/2008JB006271

Dieterich, J. H. (2007). Application of rate and state dependent friction to models of fault slip and earthquake occurrence. In: *Earthquake Seismology,* eds. G. Schubert and H. Kanimori, *Treatise on Geophysics,* vol. 4, 107 - 129

di Toro, G., R. Han, T. Hirose, N, de Paola, S. Nielsen, K. Mizoguchi, F. Ferri, M. Cocco, and T. Shimamoto (2011). Fault lubrication during earthquakes. *Nature*, *471*(7339), 494–499. doi.:10.1038/nature09838

Daub, E. G., and J. M. Carlson (2010). Friction, fracture, and earthquakes. *Annual Review of Condensed Matter Physics*, *1*, 397–418. doi:10.1146/annurev-conmatphys-070909-104025

Dunham, E. M. (2007). Conditions governing the occurrence of super shear ruptures under slip-weakening friction, *J. Geophys. Res*., 112(B7), 1–24, doi:10.1029/2006JB004717

Dunham, E. M., D. Belanger, L. Cong, and J. E. Kozdon (2011). Earthquake ruptures with strongly rate-weakening friction and off-fault plasticity, part 2: Nonplanar faults. *Bulletin of the Seismological Society of America*, *101*(5), 2308–2322. doi:10.1785/0120100076

Durran, D. R. (1999). Numerical Methods for Wave Equations in Geophysical Fluid Dynamics. New York: Springer-Verlag, ISBN 0-387-98376-7, 465 p.

Erickson, B. A., and E. M. Dunham (2014). An efficient numerical method for earthquake cycles in heterogeneous media: Alternating subbasin and surface-rupturing events on faults crossing a sedimentary basin, *J. Geophys. Res.,* 119, no. 4, 3290–3316, doi:10.1002/2013JB010614.

Erickson, B. A., J. Jiang, M. Barall, N. Lapusta, E. M. Dunham, R. Harris, L. S. Abrahams, K. L. Allison, J. P. Ampuero, S. Barbot, C. Cattania, A. Elbanna, Y. Fialko, B. Idini, J. E. Kozdon, V. Lambert, Y. Liu, B. Luo, X. Ma, M. B. McKay, P. Segall, P. Shi, M. van den Ende, and M. Wei (2020). The community code verification exercise for Simulating Sequences of Earthquakes and Aseismic Slip (SEAS). *Seismological Research Letters*, *91*(2A), 874–890. doi:10.1785/0220190248

Fang, Z., and E. M. Dunham (2013). Additional shear resistance from fault roughness and stress levels on geometrically complex faults. *Journal of Geophysical Research: Solid Earth*, *118*, doi:10.1002/jgrb.50262

Gabuchian, V., A. J. Rosakis, H. S. Bhat, R. Madariaga, and H. Kanamori (2017). Experimental evidence that thrust earthquake ruptures might open faults. *Nature*, *545*(7654), 336–339. doi:10.1038/nature22045

Gabriel, A.-A., J.-P. Ampuero, L. A. Dalguer, and P. M. Mai (2012). The transition of dynamic rupture modes in elastic media under velocity-weakening friction, *J. Geophys. Res*.,117(B9), 0148–0227, doi:10.1029/2012JB009468

Gabriel, A. A., J. P. Ampuero, L. A. Dalguer, and P. M. Mai (2013). Source properties of dynamic rupture pulses with off-fault plasticity. *Journal of Geophysical Research: Solid Earth*, *118*, 4117–4126. doi:10.1002/jgrb.50213

Galis, M., C. Pelties, J. Kristek, P. Moczo, J.-P. Ampuero, and P. M. Mai (2015). On the initiation of sustained slip-weakening ruptures by localized stresses. *Geophysical Journal International*, *200*(2), 888–907. doi:10.1093/gji/ggu436

Gallovič, F., L. Valentová, J.-P. Ampuero, A-A. Gabriel. (2019). Bayesian Dynamic Finite-Fault Inversion: 2. Application to the 2016 Mw6.2 Amatrice, Italy, Earthquake, *J. Geophys. Res. Solid Earth* 124, 6970-6988. **doi:10.1029/2019JB017512**

Gallovič, F., J. Zahradník, V. Plicka, E. Sokos, C. Evangelidis, I. Fountoulakis, and F. Turhan (2020). Complex rupture dynamics on an immature fault during the 2020 Mw 6.8 Elazığ earthquake, Turkey, *Commun. Earth Environ.* 1, 40, doi: 10.1038/s43247-020-00038-x

Geuzaine, C., and J. F. Remacle (2009). *Gmsh: a three-dimensional finite element mesh generator with built-in pre- and post-processing facilities*. International Journal for Numerical Methods in Engineering 79(11), pp. 1309-1331

Guatteri, M., and P. Spudich (2000). What can strong-motion data tell us about slip-weakening fault-friction laws? *Bulletin of the Seismological Society of America*, *90*(1), 98–116. doi:10.1785/0119990053

Guatteri, M., P. M. Mai, G. C. Beroza, and J. Boatwright (2003). Strong Ground-Motion Prediction from Stochastic-Dynamic Source Models. *Bulletin of the Seismological Society of America*, 93 (1): 301–313. doi: 10.1785/0120020006

Harris, R.A., and S. M. Day (1993). Dynamic of fault interaction: parallel strike-slip faults. *J. Geophys. Res.*, *98*(No. B3), 4461–4472. doi:10.1029/92JB02272

Harris, R.A., and S. M. Day (1997). Effects of a low-velocity zone on a dynamic rupture, *Bull. Seism. Soc. Am.*, 87, 1267-1280. doi:10.1785/BSSA0870051267

Harris, R. A., J. F. Dolan, R. Hartleb, and S. M. Day (2002). The 1999 İzmit, Turkey, earthquake: A 3D dynamic stress transfer model of intra earthquake triggering, *Bull. Seismol. Soc. Am.* 92, no. 1, 245– 255, doi: 10.1785/0120000825.

Harris, R.A., M. Barall, R. Archuleta, E. Dunham, B. Aagaard, J.P. Ampuero, H. Bhat, V. Cruz-Atienza, L. Dalguer, P. Dawson, S. Day, B. Duan, G. Ely, Y. Kaneko, Y. Kase, N. Lapusta, Y. Liu, S. Ma, D. Oglesby, K. Olsen, A. Pitarka, S. Song, and E. Templeton (2009). The SCEC/USGS Dynamic Earthquake Rupture Code Verification Exercise, *Seism. Res. Lett.* 80(1), 119-126, doi:10.1785/gssrl.80.1.119.

Harris, R.A., M. Barall, D.J. Andrews, B. Duan, E.M. Dunham, S. Ma, A.-A. Gabriel, Y. Kaneko, Y. Kase, B. Aagaard, D. Oglesby, J.-P. Ampuero, T.C. Hanks, and N. Abrahamson

(2011). Verifying a computational method for predicting extreme ground motion, *Seism. Res. Lett.* 82(5), 638-644, doi:10.1785/gssrl.82.5.638.

Harris, R. A., B. Aagaard, M. Barall, S. Ma, D. Roten, K. Olsen, B. Duan, D. Liu, B. Luo, K. Bai, J. P. Ampuero, Y. Kaneko, A. A. Gabriel, K. Duru, T. Ulrich, S. Wollherr, Z. Shi, E. Dunham, S. Bydlon, … L. Dalguer (2018). A suite of exercises for verifying dynamic earthquake rupture codes. *Seismological Research Letters*, *89*(3), 1146–1162. doi: 10.1785/0220170222

Harris, R. A., M. Barall, D. A. Lockner, D. E. Moore, D. A. Ponce, R. W. Graymer, G. Funning, C. Morrow, C. Kyriakopoulos, and D. Eberhart-Phillips (2021). A geology and geodesy based model of dynamic earthquake rupture on the Rodgers Creek-Hayward-Calaveras fault system, California. *Journal of Geophysical Research: Solid Earth*, 126, e2020JB020577. doi:10.1029/2020JB020577

Haskell, N. A. (1964). Total energy and energy spectral density of elastic wave radiation from propagating faults. *Bulletin of the Seismological Society of America*, 54, 1811 - 1841. doi: 10.1785/BSSA05406A1811

Heaton, T. (1990). Evidence for and implications of self-healing pulses of slip in earthquake rupture. *Phys. Earth. Planet. Inter.*, 64, 1 – 20. doi:10.1016/0031-9201(90)90002-F

Herrera, C., S. Ruiz, R. Madariaga, and P. Poli (2017). Dynamic inversion of the 2015 Jujuy earthquake and similarity with other intraslab events. *Geophys. J. Int.*, 209, 866–875. doi: 10.1093/gji/ggx056

Hok, S., E. Fukuyama, and C. Hashimoto (2011). Dynamic rupture scenarios of anticipated Nankai-Tonankai earthquakes, southwest Japan. *Journal of Geophysical Research: Solid Earth*, *116*(12), 1–22. doi:10.1029/2011JB008492

Huang, Y., and J. P. Ampuero (2011). Pulse-like ruptures induced by low-velocity fault zones. *Journal of Geophysical Research: Solid Earth*, *116*(12), 1–13. doi:10.1029/2011JB008684

Huang, Y., J. P. Ampuero, and D. Helmberger (2014). Earthquake ruptures modulated by waves in damaged fault zones. *Journal of Geophysical Research: Solid Earth*, *119*, 3133–3154. doi:10.1002/2013JB010724

Huang, Y. (2018). Earthquake Rupture in Fault Zones With Along-Strike Material Heterogeneity. *Journal of Geophysical Research: Solid Earth*, 9884–9898. doi:10.1029/2018JB016354

Huang, Y. (2021). Smooth Crustal Velocity Models Cause a Depletion of High-Frequency Ground Motions on Soil in 2D Dynamic Rupture Simulations. *Bulletin of the Seismological Society of America*, *111*(4), 2057–2070. doi:10.1785/0120200311

Igel, H. (2017). Computational Seismology: A Practical Guide. Oxford: Oxford University Press.

Ji, C., D.J. Wald, and D.V. Helmberger (2002). Source description of the 1999 Hector Mine, California earthquake; Part I: Wavelet domain inversion theory and resolution analysis, *Bull. Seism. Soc. Am.,* Vol 92, 4, 1192-1207. doi:10.1785/0120000916

Jiang, J., B. Erickson., V. Lambert, J. P. Ampuero, R. Ando, S. Barbot, C. Cattania, L. Dal Zilio, B. Duan, E. M. Dunham, A-A. Gabriel, N. Lapusta, D. Li, M. Li, D. Liu, Y. Liu, S. Ozawa, C. Pranger, Y. van Dinther (2022). Community-Driven Code Comparisons for Three-Dimensional Dynamic Modeling of Sequences of Earthquakes and Aseismic Slip. *Journal of Geophysical Research: Solid Earth*, 127, doi: 10.1029/2021JB023519

Kanamori, H. (1981). The nature of seismicity patterns before large earth-quakes, in Earthquake Prediction—An International Review, Maurice Ewing Series 4, D. W. Simsone and P. G. Richards (Editors), American Geophysical Union, Washington, D.C., 1–19

Käser, M., and M. Dumbser (2006). An arbitrary high-order discontinuous Galerkin method for elastic waves on unstructured meshes - I. The two-dimensional isotropic case with external source terms. *Geophysical Journal International*, *166*(2), 855–877. doi:10.1111/j.1365-246X.2006.03051.x

Krenz L., C. Uphoff, T. Ulrich, A.-A. Gabriel, L. S. Abrahams, E. M. Dunham, and M. Bader (2021). 3D Acoustic-Elastic Coupling with Gravity: The Dynamics of the 2018 Palu, Sulawesi Earthquake and Tsunami. In SC'21: The International Conference for High Performance Computing, Networking, Storage, and Analysis, Nov 14–19, 2021, St. Louis, MO. ACM, New York, NY, USA, 13 pages. https://doi.org/10.1145/1122445.1122456

Komatitsch, D., and J. Tromp (2003). A perfectly matched layer absorbing boundary condition for the second-order seismic wave equation, *Ge-phys. J. Int*.,154,146–153

Kostrov, B. V. (1964). Self-similar problems of the propagation of shear cracks. *J. Appl. Math. Mech.*, 28, 1077 - 1087. doi: 10.1016/0021-8928(64)90010-3

Kostrov, B. V. (1975). On the crack propagation with variable velocity. *Int. J. Fracture*, 11, 47 - 56. doi:10.1016/0021-8928(74)90047-1

Kozdon, J. E., and E. M. Dunham (2013). Rupture to the Trench: Dynamic rupture simulations of the 11 March 2011 Tohoku earthquake. *Bulletin of the Seismological Society of America*, *103*(2 B), 1275–1289. doi:10.1785/0120120136

Knopoff, L., and M. Randall (1970). The compensated linear vector dipole: a possible mechanism for deep earthquakes. *Journal of Geophysical Research.* 75, 4957 – 4963. **doi:10.1029/JB075i026p04957**

Kyriakopoulos, C., B. Wu, and D. D. Oglesby (2021). Asymmetric Topography Causes Normal Stress Perturbations at the Rupture Front: The Case of the Cajon Pass. *Geophysical Research Letters*, *48*(20). doi:10.1029/2021GL095397

Lamb, H. (1904). On the propagation of tremors over the surface of an elastic solid. *Phil. Trans. R. Soc. Lond. A.,* 203, 1–42. doi:10.1098/rsta.1904.0013

Lapusta, N., J. R. Rice, Y. Ben-Zion, and G. Zheng (2000). Elastodynamic analysis for slow tectonic loading with spontaneous rupture episodes on faults with rate- and state-dependent friction. *Journal of Geophysical Research: Solid Earth*, *105*(B10), 23765–23789. doi:10.1029/2000JB900250

Lapusta, N., and Y. Liu (2009). Three-dimensional boundary integral modeling of spontaneous earthquake sequences and aseismic slip, *J. Geophys. Res*. 114, no. B9, doi: 10.1029/2008JB005934.

Lotto, G. C., and E. M. Dunham (2015). High-order finite difference modeling of tsunami generation in a compressible ocean from offshore earthquakes. *Comp. Geosci.*, 19(2), 327–340. doi:10.1007/s10596-015-9472-0

Lozos, J. C., and R. A. Harris (2020). Dynamic Rupture Simulations of the M6.4 and M7.1 July 2019 Ridgecrest, California, Earthquakes. *Geophysical Research Letters*, *47*(7), 1–9. doi: 10.1029/2019GL086020

Ma, S., and D. J. Andrews (2010). Inelastic off-fault response and three-dimensional earthquake rupture dynamics on a strike-slip fault, *J. Geophys. Res., 115,* B04304, doi:10.1029/2009JB006382

Ma, X., S. Hajarolasvadi, G. Albertini, D. S. Kammer, and A. E. Elbanna (2019). A hybrid finite element-spectral boundary integral approach: applications to dynamic rupture modeling in unbounded domains. *Int J Numer Anal Methods Geomech.* 43(1), 317-338. doi: 10.1002/ nag.2865

Madariaga, R. (1976). Dynamics of an expanding circular fault. *Bull. Seismo. Soc. Am.,* 66, 639–666. doi:10.1785/BSSA0660030639

Madariaga, R., and K. B. Olsen (2002). Earthquake Dynamics. *International Handbook of Earthquake and Engineering Seismology*, *81A*, 175–194.

Madariaga, R., and S. Ruiz (2016). Earthquake dynamics on circular faults: a review 1970 – 2015. *Journal of Seismology*, *20*, 1235–1252. doi:10.1007/s10950-016-9590-8

Madden, E. H., M. Bader, J. Behrens, Y. van Dinther, A. A. Gabriel, L. Rannabauer, T. Ulrich, C. Uphoff, S. Vater, and I. van Zelst (2020). Linked 3-D modelling of megathrust earthquake-tsunami events: From subduction to tsunami run up. *Geophysical Journal International*, *224*(1), 487–516. doi: 10.1093/gji/ggaa484

Mai, P. M., V. Jagdish, A.-A. Gabriel, and T. Ulrich (2021). Earthquake rupture properties in presence of thermal-pressurization of pore fluids. *EGU abstract*. 2021EGUGA..2315202M

Marone, C., and D. M. Saffer (2007). Fault Friction and the Upper Transition from Seismic to Aseismic Faulting. *The Seismogenic Zone of Subduction Thrust Faults*, *chp. 12*, 346-369. doi: 10.7312/dixo13866-012

Moczo, P., J. Kristek, and M. Galis (2014). The Finite Difference Modeling of Earthquake Motion. Cambridge: Cambridge University Press.

Moore, D. E., D. A. Lockner, and S. Hickman (2016). Hydrothermal frictional strengths of rock and mineral samples relevant to the creeping section of the San Andreas Fault. Journal of Structural Geology, 89, 153–167. doi:10.1016/J.JSG.2016.06.005

Morrow, C. A., D. E. Moore, and D. A. Lockner (2010). Dependence of frictional strength on compositional variations of Hayward fault rock gouges, Proceedings of the Third Conference on

Earthquake Hazards in the Eastern San Francisco Bay Area. California Geological Survey Special Report, 219, 115–127.

Nakano, H. (1923). Notes on the nature of forces which give rise to earthquakes motion. *Seis. Bull. Cent. Meteor. Obs. Japan*, 1, 92 - 120.

Noda, H., E. M. Dunham, and J. R. Rice (2009). Earthquake ruptures with thermal weakening and the operation of major faults at low overall stress levels, *J. Geophys. Res.,* 114, B07 302, doi:10.1029/2008JB006143

Oglesby, D. D., and S. M. Day (2002). Stochastic fault stress: Implications for fault dynamics and ground motion, *Bull. Seismol. Soc. Am*, 92, no. 8, 3006–3021, doi:10.1785/0120010249

Okada, Y. (1985). Surface deformation due to shear and tensile faults in a half-space. *Bulletin of the Seismological Society of America*, *23*(4), 128. doi:10.1016/0148-9062(86)90674-1

Okubo, P. G., and J. H. Dieterich (1984). Effects of physical fault properties on frictional instabilities produced on simulated faults. *Journal of Geophysical Research*, *89*(B7), 5817–5827. doi:10.1029/JB089iB07p05817

Olsen, K. B., Simulation of three dimensional wave propagation in the Salt Lake Basin, Ph.D. thesis, The University of Utah, Salt Lake City, Utah, 1994.

Pelties, C., J. de La Puente, J. P. Ampuero, G. B. Brietzke, and M. Käser (2012), Three-dimensional dynamic rupture simulation with a high-order discontinuous Galerkin method on unstructured tetrahedral meshes. *Journal of Geophysical Research: Solid Earth*, *117*(2), 1–15. doi:10.1029/2011JB008857

Power, W. L., and T. E. Tullis (1991), Euclidean and fractal models forthe description of rock surface roughness, *J. Geophys. Res*.,96(B1),415–424, doi:10.1029/90JB02107

Premus, J., F. Gallovič, L. Hanyk, L., and A.-A. Gabriel (2020). FD3D_TSN: Fast and simple code for dynamic rupture simulations with GPU acceleration. *Seismological Research Letters*. doi:10.1785/0220190374.

Pujol, J., and R. B. Herrmann (1990). A student's guide to point sources in homogeneous media, *Seism. Res. Letters*, 61, 209-224. doi:10.1785/gssrl.61.3-4.209

Ramos, M. D and Y. Huang (2019). How the transition region along the Cascadia megathrust influences coseismic behavior: Insights from 2-D dynamic rupture simulations. *Geophysical Research Letters*, *46*, 1–11. doi:10.1029/2018gl080812

Ramos, M. D., Y. Huang, T. Ulrich, D. Li, A-A. Gabriel, and A. M. Thomas (2021). Assessing Margin-Wide Rupture Behaviors Along the Cascadia Megathrust With 3-D Dynamic Rupture Simulations. *Journal of Geophysical Research: Solid Earth*, *126*(7). doi:10.1029/2021JB022005

Rice, J. R. (1993). Spatio-temporal Complexity of Slip on a Fault. *Jour. of Geophys Res.*, 98, 9885-9907. **doi:10.1029/93JB00191**

Rice, J. R. (1992). Fault Stress States, Pore Pressure Distributions, and the Weakness of the San Andreas Fault. *International Geophysics*, *51*(C), 475–503. doi:10.1016/S0074-6142(08)62835-1

Ripperger, J., and P. M. Mai (2004). Fast computation of static stress changes on 2D faults from final slip distributions. *Geophysical Research Letters*, *31*(18), 2–5. doi:10.1029/2004GL020594

Roten, D., Y. Cui, K. B. Olsen, S. M. Day, K. Withers, W. H. Savran, P. Wang, and D. Mu (2016). High-frequency nonlinear earthquake simulations on petascale heterogeneous supercomputers, *Proc. Supercomputing Conference*, Salt Lake City, Utah, November 2016

Rowe, C. D., J. C. Moore, J. C., and F. Remitti (2013). The thickness of subduction plate boundary faults from the seafloor into the seismogenic zone. *Geology*, *41*(9), 991–994. doi:10.1130/G34556.1

Roten, D., K. B. Olsen, and S. M. Day (2017). Off-fault deformation and shallow slip deficit from dynamic rupture simulations with fault zone plasticity, *Geophys. Res. Lett*., 44, 7733–7742, doi:10.1002/2017GL07432

Rubin, A. M., and J. P. Ampuero (2005). Earthquake nucleation on (aging) rate and state faults. *Journal of Geophysical Research: Solid Earth*, *110*(B11312). doi:1029/2005JB003686

Ryan, K. J., and D. D. Oglesby (2014). Dynamically modeling fault step overs using various friction laws. *Journal of Geophysical Research: Solid Earth*, *119*(7), 5814–5829. doi:10.1002/2014JB011151

Ryan, K. J., and D. D. Oglesby (2017). Modeling the effects of a normal-stress-dependent state variable, within the rate-and state-dependent friction framework, at stepovers and dip-slip faults. *Pure and Applied Geophysics*, *174*(3), 1361-1383. doi:10.1007/s00024-017-1469-2

Savran, W. H. and K. B. Olsen (2020). Kinematic rupture generator based on 3-D spontaneous rupture simulations on geometrically rough faults. *Journal of Geophysical Research: Solid Earth*, 125, e2020JB019464. doi:10.1029/2020JB019464

SIMetrix Simulator Reference Manual, version 8.1, SIMetrix Tecnologies Ltd., Oct. 2016. Accessed on: Nov. 15, 2021. [Online]. Available: https://www.simetrix.co.uk/Files/manuals/8.1/SimulatorReference.pdf

Small, P., D. Gill, P. J. Maechling, R. Taborda, S. Callaghan, T. H. Jordan, G. P. Ely, K. B. Olsen, and C. A. Goulet (2017). The SCEC Unified Community Velocity Model Software Framework. Seismological Research Letters, 88(5). doi:10.1785/0220170082.

Stephenson, W. J., N. G. Reitman, S. J. Angster, S. J. (2017). P- and S-wave velocity models incorporating the Cascadia subduction zone for 3D earthquake ground motion simulations. *USGS Open File Report*, *December*, 28. doi:10.3133/ofr20171152

Thakur, P., Y. Huang, and Y. Kaneko (2020). Effects of Low-Velocity Fault Damage Zones on Long-Term Earthquake Behaviors on Mature Strike-Slip Faults. *Journal of Geophysical Research: Solid Earth*, *125*(8), 1–20. doi:10.1029/2020JB019587

Thomas, M. Y., N. Lapusta, H. Noda, and J.-P. Avouac (2014). Quasi-dynamic versus fully-dynamic simulations of earthquakes and aseismic slip with and without enhanced coseismic weakening, Journal of Geophysical Research-solid Earth, 119, 1986-2004. doi:10.1002/2013JB010615

Ulrich, T., A. A. Gabriel, J. P. Ampuero, and W. Xu (2019). Dynamic viability of the 2016 Mw 7.8 Kaikōura earthquake cascade on weak crustal faults. *Nature Communications*, *10*(1). doi:10.1038/s41467-019-09125-w

van Zelst, I., S. Wollherr., A. A. Gabriel, E. H. Madden, and Y. van Dinther (2019). Modeling Megathrust Earthquakes Across Scales: One-way Coupling from Geodynamics and Seismic Cycles to Dynamic Rupture. *Journal of Geophysical Research: Solid Earth*, *124*(11), 11414–11446. doi: 10.1029/2019JB017539

Wallace, R. E. (1970). Earthquake Recurrence Intervals on the San Andreas fault. *GSA Bulletin*. 81 (10). 2875 – 2890. doi: 10.1130/0016-7606(1970)81[2875:ERIOTS]2.0.CO;2

Weng, H., and J. P. Ampuero (2020). Continuum of earthquake rupture speeds enabled by oblique slip. *Nature Geoscience*, *13*(12), 817–821. doi:10.1038/s41561-020-00654-4

Wilson, A., and S. Ma (2021). Wedge Plasticity and Fully Coupled Simulations of Dynamic Rupture and Tsunami in the Cascadia Subduction Zone. *Journal of Geophysical Research: Solid Earth*, *126*(7). doi:10.1029/2020JB021627

Aniko Wirp, S., A. -A. Gabriel, M. Schmeller, E. H. Madden, I. van Zelst, L. Krenz, Y. van Dinther, and L. Rannabauer (2021). 3D Linked Subduction, Dynamic Rupture, Tsunami, and

Inundation Modeling: Dynamic Effects of Supershear and Tsunami Earthquakes, Hypocenter Location, and Shallow Fault Slip. *Frontiers in Earth Science*, *9*. Doi:10.3389/feart.2021.626844

Wollherr, S., A.-A. Gabriel, and C. Uphoff (2018). Off-fault plasticity in three-dimensional dynamic rupture simulations using a modal Discontinuous Galerkin method on unstructured meshes: implementation, verification and application. *Geophysical Journal International*, *214*(3), 1556–1584. doi:10.1093/gji/ggy213

Wollherr, S., A. A. Gabriel, and P. M. Mai (2019). Landers 1992 "Reloaded": Integrative Dynamic Earthquake Rupture Modeling. *Journal of Geophysical Research: Solid Earth*. doi:10.1029/2018JB016355

Yang, H., S. Yao, B. He, A. Newman, and H. Weng (2019). Deriving rupture scenarios from interseismic locking distributions along the subduction megathrust. *Journal of Geophysical Research: Solid Earth*, 2019JB017541. doi:10.1029/2019JB017541

Yin, J., and M. A. Denolle (2021). The Earth's Surface Controls the Depth-Dependent Seismic Radiation of Megathrust Earthquakes. *AGU Advances*, *2*(3). doi:10.1029/2021av000413

Zhang, W., T. Iwata, K. Irikura, H. Sekiguchi, and M. Bouchon (2003). Heterogeneous distribution of the dynamic source parameters of the 1999 Chi-Chi, Taiwan, earthquake, *J. Geophys. Res.*, 108(B5), 2232, doi:10.1029/2002JB001889

Zhang, Z., W. Zhang, D. Xin, K. Chen, and X. Chen (2021). A dynamic-rupture model of the 2019 Mw 7.1 Ridgecrest earthquake being compatible with the observations. *Seismological Research Letters*, *92*(2), 870–876. doi:10.1785/0220200258

Table 1. Nomenclature

Common Terms used in Dynamic Rupture Models	
Term	*Definition*
Cohesive Zone (Λ)	An area behind the rupture-front where fault strengths decrease from their static to dynamic level – a fundamental length scale in dynamic rupture models.
Crack-like Rupture	A rupture model where the rise time is comparable to the total rupture duration.
Critical Slip Distance (D_c)	The slip needed for fault strength to drop from static level to dynamic level.
Cut-off Velocity (V_c)	A critical velocity scale in velocity-weakening friction laws that controls the steady-state frictional behavior.
Dynamic Fault Strength	The fault strength right during slip; is the product of the effective normal stress and the dynamic friction coefficient. $\sigma_d = \sigma_n^{eff} \cdot \mu_{dynamic}$
Dynamic Stress Drop ($\Delta\sigma_d$)	The difference in shear stress before and <u>during</u> an earthquake.
Effective Normal Stress	The difference between lithostatic and pore pressure (p) operating on a fault. $\sigma_n^{eff} = \sigma_n - p$
Fracture Energy (E_G)	The energy needed to grow a propagating shear crack. If the slip-weakening friction law is used, this energy is $E_G = {}^1/_2 \cdot (\sigma_s - \sigma_d) \cdot D_c$

Pulse-like Rupture	A rupture model where the rise time is much shorter than the total rupture duration.
Rise Time	The time it takes for a point on the fault to reach its largest value. Not necessarily equal to the duration of rupture.
Slip	The relative displacement at a given location on the fault.
Static Fault Strength	The fault strength right before it starts moving; it is the product of the effective normal stress and the static friction coefficient. $\sigma_s = \sigma_n^{eff} \cdot \mu_{static}$
Static Stress Drop ($\Delta\sigma_s$)	The difference in shear stress before and after an earthquake. Its spatial average over the area of the fault that slipped (A) is given by $\Delta\sigma_s \cong \overline{\Delta\sigma_s} = \frac{1}{A}\int \Delta\sigma_s dA$
Strength Drop (Strength Excess)	The difference between static strength and dynamic strength.